Journal of Scientific Research & Reports
3(1): 204-226, 2014; Article no. JSRR.2014.010

SCIENCEDOMAIN *international*
www.sciencedomain.org

Ionospheric Anomaly after the 11 April, 2012, M_w=8.6 Indonesia' Sumatra Earthquake Using Two-Dimensional Principal Component Analysis (2DPCA)

Jyh-Woei Lin[1*]

[1]*Department of Earth Science, National Cheng Kung University, No.1 University Road, Tainan City, Taiwan.*

Author's contribution

This whole work was carried out by the author.

Research Article

Received 9th July 2013
Accepted 3rd September 2013
Published 17th October 2013

ABSTRACT

Two-dimensional Principal Component Analysis (2DPCA) and principal component analysis (PCA) were performed to determine two-dimensional ionospheric total electron content (TEC) anomaly after Indonesia's Sumatra earthquake on 11 April, 2012 (UT) (M_w =8.6). The earthquake occurred at 08:38:37UT with vibrated duration time of 2 minutes and therefore the TEC data at the time 08:40 to 08: 50 (UT) after the earthquake were examined using both PCA and 2DPCA. The TEC anomaly was more intense localized at 08:40 to 08: 45 (UT) but the range was outside the epicenter. Potential cause of the TEC anomaly, which may be a density variance, was rising high speed slanted acoustic shock wave, which had small horizontal component, resulted by the mainshock of the earthquake. The duration time of this TEC anomaly was at least 5 minutes.

Keywords: Two-dimensional Principal Component Analysis (2DPCA); Principal Component analysis (PCA); two-dimensional Total Electron Content (TEC); Indonesia's Sumatra earthquake; slanted acoustic shock waves.

**Corresponding author: E-mail: pgjwl1966@gmail.com;*

1. INTRODUCTION

TEC anomalies associated with large earthquakes have been widely researched both as precursors and aftereffects [1,10,15,24,25,26,27,31,33,35,37,39]. The exact causes of earthquake associated precursor TEC anomalies are not known; however, there are many possibilities including gravity waves generated by the solid-earth and sea, as well as lower atmospheric electric fields resulting from earthquake preparation processes that can be transferred into the ionosphere along geomagnetic lines [34]. Regardless of the specific causes of earthquake-precursor TEC anomalies, their earthquake association has been established statistically using deviations from running TEC median values after eliminating other possible causes of TEC disturbance such as solar flare and geomagnetic storm activity [22]. The TEC anomalies are most likely caused by acoustic gravity waves traveling from the earth's surface into the ionosphere [2,10,26,27,31]. The mechanism for this is thought to be earth's atmosphere acting as a natural amplifier. During an earthquake tiny amounts of kinetic energy are transferred from the solid earth to the lower atmosphere. If this kinetic energy is conserved, then given the exponential decline in atmospheric density with height, waves of great amplitude can result in the ionosphere. It has been estimated that millimeter disturbances at the earth's surface can be amplified to waves of amplitude 100 m at 100 km altitude [26]. [26] has used ground based receivers to detect post-seismic ionospheric disturbance using global positioning system (GPS) satellites found that the measurable impact of the gravity waves resulting from the Nov. 3. Denali, Alaska M=7.9 earthquake produced small but detectable changes in the TECu count of 0.1% peak to peak. This disturbance was detected by 6 other satellites. [26] also measured the effects of near field seismic waves for the Hokkaido earthquake of Sept. 25, 2003 (M_w =8.3). In that experiment, they found that acoustic waves could be detected as high as 800 km, they also measured the gravity wave impact for the same earthquake and got similar results to those for the Alaskan Denlai earthquake in terms of TECu disturbance. One issue, however, with all TEC measurement is the nature of the ionosphere. The electron content of the ionosphere is highly dynamic plasma so that establishing anomalies and event association is not easy. For example, determining a running median of TEC content before large earthquakes to search for precursor TEC anomalies is difficult and may not always be reliable because TEC can be affected by many factors. [34] makes an extensive list of possible causes, including radon gas release, causing lower atmospheric electric fields which travel up into the ionosphere along geomagnetic lines while [8] suggests P-type semiconductor effect as the cause of lower atmosphere electric fields. P-type semiconductor effect, whereby charge separation occurs in metamorphic, near-cracked and igneous rock between electrons in the stressed range of rock and small positive holes occurring away from stressed regions. Once the positive holes are generated some phenomena occur as current propagates through rocks resulting in electromagnetic emissions. Recent studies have shown that earthquake-associated TEC anomalies are detectable using principal component analysis (PCA) [22]. PCA is an alternative pure mathematical method for the measuring TEC anomalies. The method relies on exploiting signal delay between GPS satellites and ground receiver stations without direct observation of ionospheric TEC. The long term period variance of ionospheric TEC [22] does not affect the outcome of the results using PCA and the potential influence of other factors such as solar flares and geomagnetic disturbance are eliminated using relevant Dst and Kp indexes statistically. The Kp index is derived by calculating a weighted average of K-indices from a network of geomagnetic observatories. Since these observatories do not report their data in real-time, various operations centers around the globe estimate the index based on data available from their local network of observatories. The Kp-index was introduced by [3]. The disturbance storm time (Dst, Kyoto Dst) index is a measure in the

context of space weather. It gives information about the strength of the ring current around earth caused by solar protons and electrons [11]. The ring current around earth produces a magnetic field that is directly opposite earth's magnetic field, i.e. if the difference between solar electrons and protons gets higher, then earth's magnetic field becomes weaker. A negative Dst value means that earth's magnetic field is weakened. This is particularly the case during solar storms. While these PCA experiments were able to detect and even described the physical shape of earthquake associated TEC anomalies, the PCA method might not be as useful as 2DPCA in the detection of TEC anomalies. 2DPCA is perform to examine the two-dimension ionospheric TEC situation after the 11 April 2012 Indonesia's Sumatra Earthquake (2.311° N, 93.06°E) at the depth of 22.9km and discuss possible cause of any discovered anomaly.

2. SOURCE DATA

The TEC data are requested from NASA Global Differential GPS system (GDGPS) from ~100 real-time GDGPS tracking sites, augmented with additional sites that are available for each 5 minutes. The integrated electron density data along each receiver-GPS satellite link is processed through a Kalman filter in a sun-fixed frame to produce the global TEC maps (GIMs). The core of the GDGPS network is the NASA Global GPS Network (GGN), a JPL-owned and operated network of roughly 70 geodetic-quality, dual frequency receivers, distributed globally. Additional real-time sites are contributed by a variety of U.S. and international partner organizations. The result is the world's largest real-time GPS tracking network, with more than 100 global sites (as of October 2006). All these sites stream their GPS measurements at 1 Hz to the GDGPS Operation Centers (GOCs), where it is processed and analyzed in real-time. The GDGPS network is highly redundant, by design, to provide a unique measure of reliability to the many critical applications that depend on it, such as real-time GPS integrity moitoring, and precise differential corrections. On average, the network is 25-fold redundant (meaning that at any given time each GPS satellite is observed, on average, by 25 ground sites), and is minimally 10-fold redundant. A veriety of communications channels are used for streaming the raw measurements from the tracking sites to the GOCs, including internet, dedicated land lines, and satellite links. When internet is used the data is sent in parallel to multiple GOCs to ensure redundancy of the internet channels. All the GOCs are inter-connected with Frame Relay or T1 lines. The GDGPS system is proud to count 4 national timing laboratories among it contributing network partners. In particular, the United States Naval Observatory (USNO) contributes two monitoring sites driven by its Master Clock, allowing the GDGPS System to provide its global users the most accurate real-time realization of USNO UTC. In addition, many GDGPS sites are driven by atomic frequency standards, enabling robust data quality schemes. Because we own and operate the vast majority of the tracking sites, we can configure the receivers to extract any and all GPS data. These include all L1 and L2 phase and pseudorange measurements, the navigation message, SNR values, and any other civilian GPS data. It typically takes about 1 second for the tracking data from most of the monitoring sites to reach the GOCs, and a few more seconds for processing and quality control. The final products, such as the precise corrections to the GPS broadcast ephemeris, are available within 5 seconds of data collection at the remote site. To ensure the integrity of the GDGPS products, the data from the GGN core of the network is authenticated. Consequently, the system is immuned to data spoofing. The extremely high redundancy of the network is another powerful measure against spoofing of data from any site, as strong majority voting schemes can be amployed to detect any anomalous sites. Processing to estimate TEC value needs to consider some biases (influences) during restore of TEC values from measurements of dual-frequency delays of GPS signals, which related with cycle slips,

resolving of carrier phase ambiguity, determination hardware delays for phase, code measurements, tropospheric and multipath problems. The Kalman filter has been used to estimate the TEC with less bias [19,26].

3. METHOD

3.1 PCA and 2DPCA

PCA is used to identify and remove correlations among problem variables so as to reduce dimensional space with less loss of information in a given dataset [6,21]. For PCA, the input data matrix is *A* which has the dimensions of $n \times m$; *S* is called the scores matrix and has dimensions of $n \times d$, where *d* is the given number of factors; *L* is called the loading matrix and it has dimensions $m \times d$ (*m*>*d*); and the matrix of residuals is called *E* with dimensions $n \times m$. The scores matrix is given by the following relation:

$$A = SB^{T} + E \tag{1}$$

Taking $B^{T}B = I$ as the unit matrix for mapping the followed form:

$$\underline{S} = \underline{A}\,L \tag{2}$$

where $\underline{S}$ is a row of *S* (a single data vector), and $\underline{A}$ is the corresponding row of *A* or the coordinates of $\underline{S}$ in the feature space. *L* is the matrix for linear transformation. By reversing the projection, then followed equation is given below:

$$\underline{A}' = \underline{S}\,L^{T} \tag{3}$$

Here $\underline{A}' = \underline{A} - \underline{E}$ is the reconstructed measurement vector, and the Euclidean norm is $\|E\|$, which must be minimized for the given number of factors. To satisfy this criterion, the columns of *R* must be the eigenvector corresponding to the *d* eigenvalues of covariance matrix of A when computed.

For 2DPCA, let signals are represented by a matrix A (the dimension of *n* x *m*). Linear projection of the form is considered as followed [20,36].

$$y = Ax \tag{4}$$

Here x is an n dimensional project axis and y is the projected feature of signals on x called principal component vector. E: is ensemble average of the elements of a vector.

$$\mathrm{W} = (y - E(y))(y - E(y))^{T} \tag{5}$$

The trace of W is defined;

$$tr(\mathrm{W}) = tr\{x^{T}Gx\}\text{, where } G = (A - E(A))(A - E(A))^{\mathrm{T}} \tag{6}$$

The matrix W is called covariance matrix of signals and the vector x maximizing Eq.6 corresponds to the largest (principal) eigenvalue of W , and the largest eigenvalue is the most dominant component of the data, therefore largest eigenvalue is represented the principal characteristics of the data [12,20,36]. PCA assigns large principal eigenvalue to the earthquake related TEC anomalies [22]. The PCA converts the measurements into one-dimensional data before covariance matrix calculation [38. The covariance matrix of PCA is based on an input matrix with the dimension of *m x n*, which is reshaped from one-dimensional data (length of m multiplying n). The spatial structure information can not be well preserved with some original information loss when inverting to original dimension under the condition of the matrix being small sample size (SSS) using PCA. Such information loss is called SSS problem (reshaping one-dimension data into SSS data to cause computed error by PCA). However, the covariance matrix in 2DPCA is full rank for a matrix of low dimension. Therefore the curse of dimensionality and SSS problem (low dimensional data problem) can be avoided [20,36]. TEC data are examined by using 2DPCA to detect earthquake-related TEC anomaly after the earthquake and the GIMs are only used to observe TEC situation in this study.

3.2 TEC Data Processing Using PCA and 2DPCA

Figure 1(a) shows the GIM (global TEC map) at the time 08:40 UT on 11 April 2012, and two equatorial ionization anomaly (EIA) crests of dense GPS TEC bands at low latitudes centered about 30°N and 10°S geographic latitudes straddle the geomagnetic equator and range from about 60°E to 130°E. The earthquake-associated TEC anomalies are not easy to observe. The TEC data of the global region (not dividing the GIM for image processing) in Figure 1(a) are divided into 600 smaller areas 12° in longitude and 9° in latitude, respectively. The spatial resolution of the TEC data for this GPS system is 5 and 2.5 degrees in longitude and latitude, respectively [4,9,16] and therefore, each small area (12° in longitude and 9° in latitude) has 4 TEC data. The TEC are anomalies usually spread widely from the epicenters of large earthquakes from the results of Lognonné et al. [17] and [26] and therefore size of an area is reasonable to detect earthquake-related TEC anomaly. The 4 TEC data form a matrix with the dimensions of 2 x 2 as small sample signal size (SSS) matrix *A* of Eq.2 and 4 for PCA and 2DPCA in each area (SSS data in each area). This allows for principal eigenvalues of and 2DPCA to be computed for each of the 600 smaller areas. The respective results of 2DPCA are given in Figure 1(b). Figure 1(c) shows principal eigenvalues of PCA related to Figure 1(a).

4. RESULTS AND DISCUSSION

Fig. 1(b) gives a color-coded scale of the magnitudes of principal eigenvalues corresponding of 2DPCA to Fig. 1(a). This global region is divided into 600 smaller areas, 12° in longitude and 9° in latitude to detect more detailed TEC situation. In an area denotes magnitude of the principal eigenvalue in this area. From this figure it can be seen that 600 principal eigenvalues are assigned. The representative of large principal eigenvalues in the Fig. 1(b) shows the existence of earthquake-related TEC anomaly represented by a large principal eigenvalue of 2DPCA. However, this TEC anomaly is found near EIA region but the anomaly range does not cover the epicenter in Fig. 1(b). Earthquake-related TEC anomaly (Fig. 1c) did not reveal and therefore 2DPCA is better than PCA to detect earthquake-associated TEC anomaly. Smaller-earthquake-related and non-earthquake TEC anomalies (e.g. the equatorial ionization anomaly (EIA)) are suppressed by large principal eigenvalues defining as earthquake-related TEC anomaly. Supposed the largest principal eigenvalue related to

the earthquake was removed, smaller-earthquake-related and non-earthquake TEC anomalies would reveal.

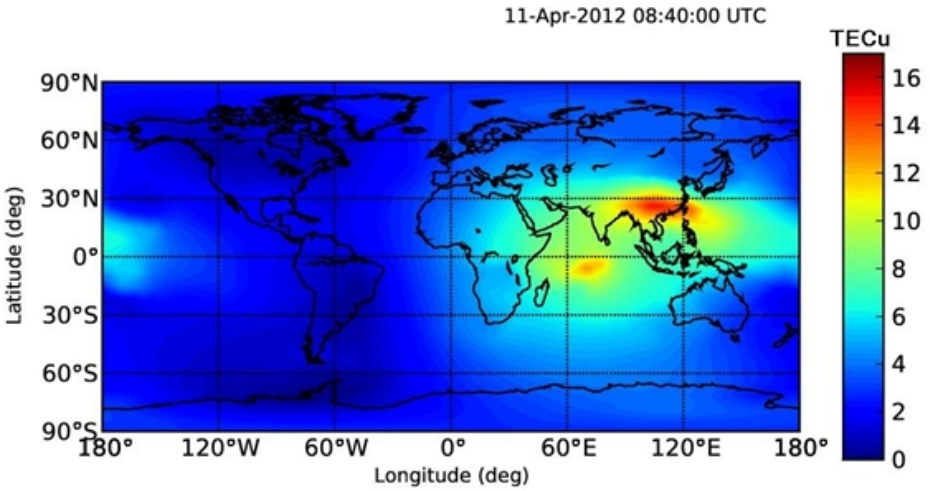

Fig. 1(a). This figure shows the GIM at the time 08:40UT on 11 April. The equatorial ionization anomaly (EIA) crests of dense GPS TEC bands at low latitudes centered about 30°N and 10°S geographic latitudes straddle the geomagnetic equator and range from about 60°E to 130°E.

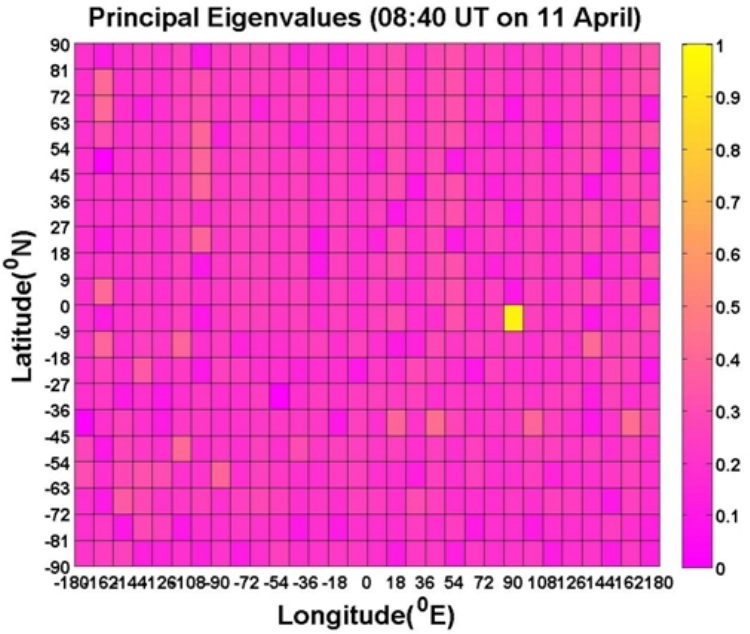

Fig. 1(b). The figure gives a color-coded scale of the magnitudes of principal eigenvalues of 2DPCA corresponding to Figure 1(a). The color within a area denotes the magnitude of a principal eigenvalue corresponding to Figure. 1(a), so that there are 600 principal eigenvalues assigned (i.e., each area in the bottom figures represents a principal eigenvalue), respectively. The earthquake-related TEC anomalies are represented using large principal eigenvalues being 0.93.

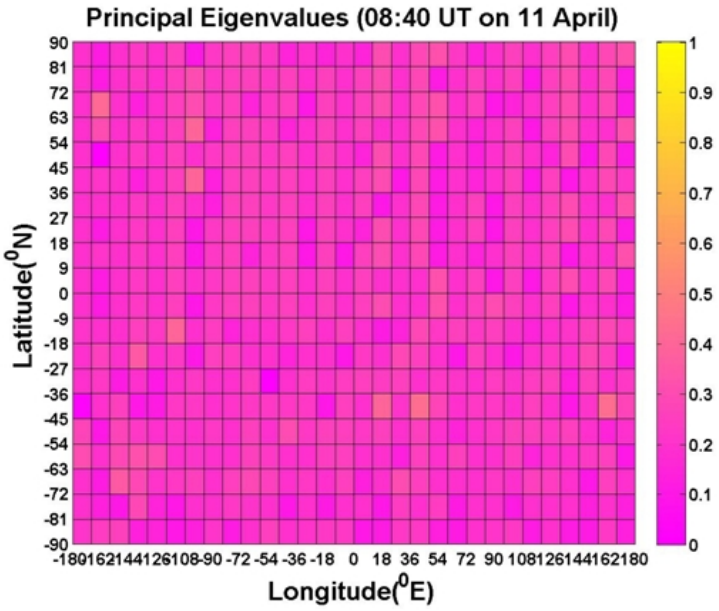

Fig. 1(c). The figure gives a color-coded scale of the magnitudes of principal eigenvalues using PCA related to Figure 1(a). Note; the principal eigenvalue has no unit. The colors of these areas seem to be uniform, and however the magnitudes have some differences.

Therefore the TEC anomaly related to this earthquake should be very large due to its large magnitude (M_w =8.6) and shallow depth (22.9km). The possibility of other factors such as solar flare and geomagnetic effects affecting the results are considered by examining Kp indices [5,13,29] in Fig. 2. The Kp index in Fig. 2. is calculated as a weighted average of K-indices from a network of geomagnetic observatories. The Kp index allows for disturbances in the horizontal component of earth's magnetic field to be represented on a scale of 0-9 with 1 being calm and 5 or more indicating a geomagnetic storm. April, 11 was geomagnetic quiet day shown in Fig. 2 (Kp$\leqq$4). 2DPCA is already expected to have well results rather than PCA.

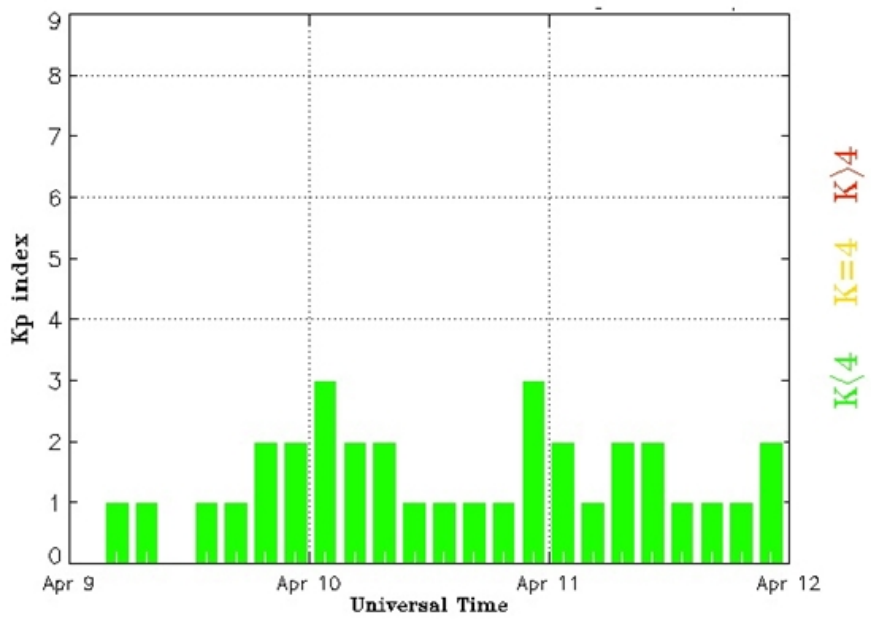

Fig. 2. This figure shows the Kp indices from 10 to 12 April 2012 (NOAA Space Weather Prediction Center).

The TEC data of the GIMs on 10 and 12, April 2012 before and after the earthquake are chosen to make comparisons with 11 April due to geomagnetic quiet days (Figure 2, Kp$\leqq$4). The three days are chosen because they should have similar non-earthquake background noises e.g. sun effects due to short time period. The TEC data of the GIMs at 08:40 to 08:50 UT on 10 April in Fig. 3(a) are examined using 2DPCA to see if TEC anomalies are detectable. The analysis results of 2DPCA are shown in Fig. 3(b). The same TEC data processing described in Section 2.2 is used to the TEC data of GIMs at 08:40 to 08:50 UT on 12 April in Fig. 4(a) shown in Figure 4(b). Earthquake-related TEC anomalies are not evident with large principal eigenvalues.

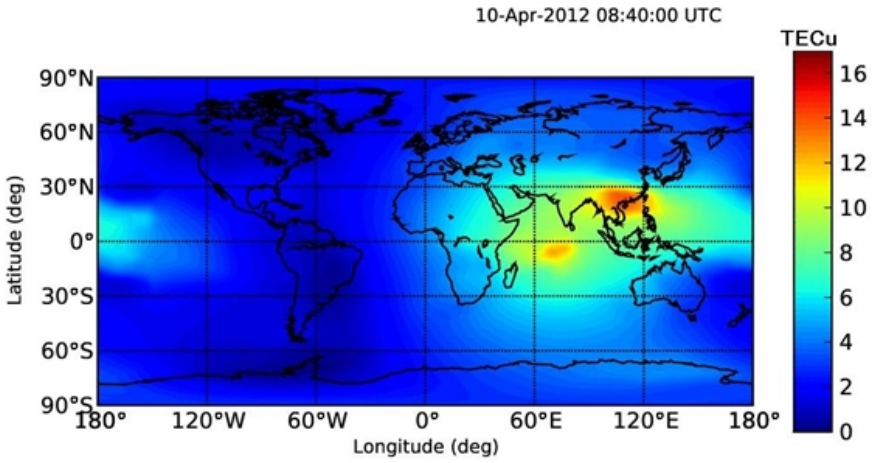

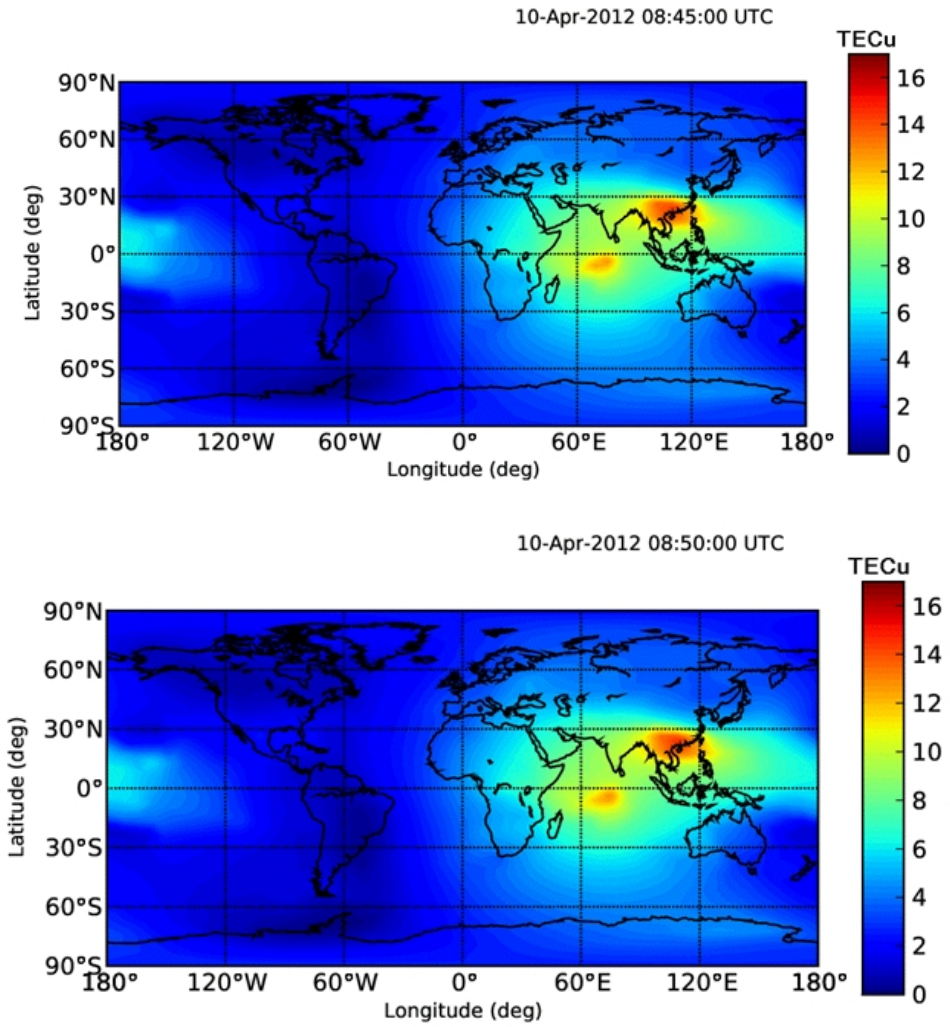

Fig. 3(a). The figures show the GIMs at the time 08:40 to 08:50 UT on 10 April 2012. The equatorial ionization anomaly (EIA) crests of dense GPS TEC bands at low latitudes centered about 30°N and 10°S geographic latitudes straddle the geomagnetic equator and range from about 60°E to 130°E.

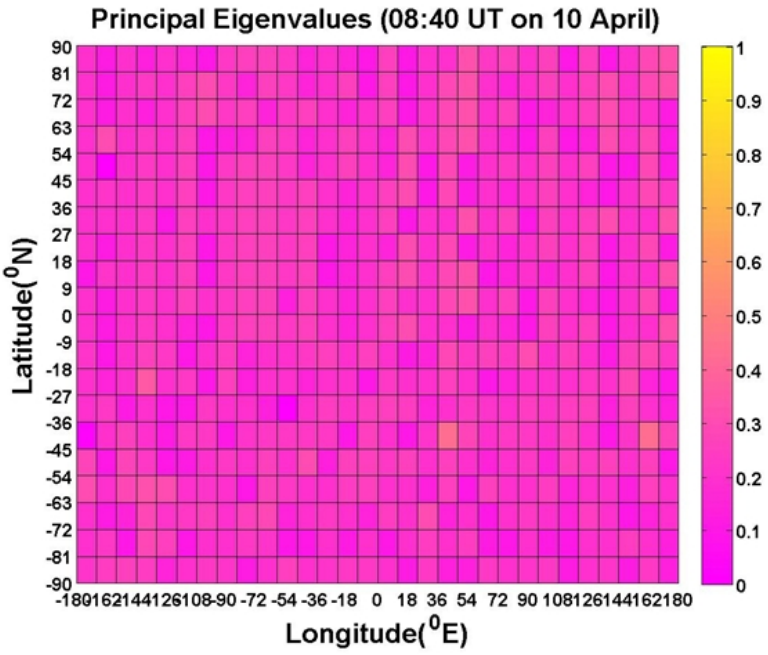
Principal Eigenvalues (08:40 UT on 10 April)
Latitude(0N)
90 81 72 63 54 45 36 27 18 9 0 -9 -18 -27 -36 -45 -54 -63 -72 -81 -90
Longitude(0E)
-180 -162 -144 -126 -108 -90 -72 -54 -36 -18 0 18 36 54 72 90 108 126 144 162 180
1 0.9 0.8 0.7 0.6 0.5 0.4 0.3 0.2 0.1 0

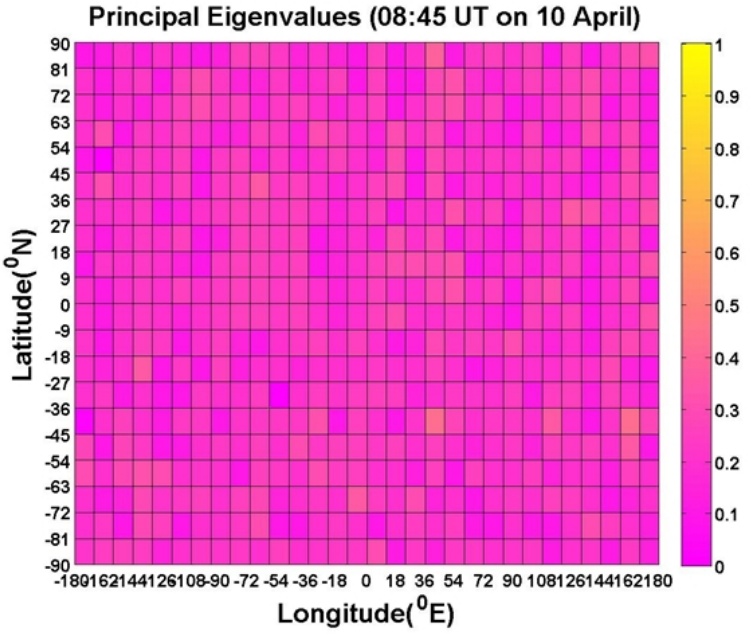
Principal Eigenvalues (08:45 UT on 10 April)
Latitude(0N)
90 81 72 63 54 45 36 27 18 9 0 -9 -18 -27 -36 -45 -54 -63 -72 -81 -90
Longitude(0E)
-180 -162 -144 -126 -108 -90 -72 -54 -36 -18 0 18 36 54 72 90 108 126 144 162 180
1 0.9 0.8 0.7 0.6 0.5 0.4 0.3 0.2 0.1 0

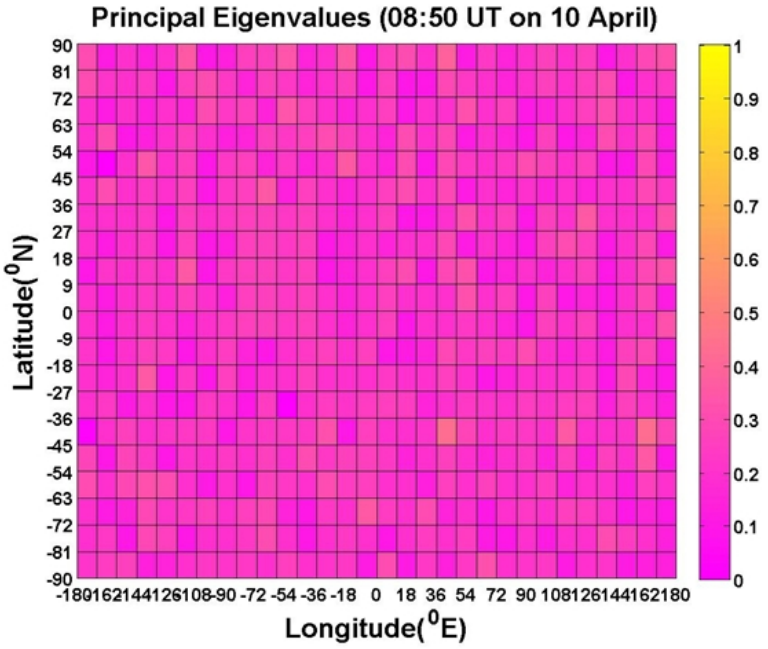

Fig. 3(b). The figures give a color-coded scale of the magnitudes of principal eigenvalues using 2DPCA related to Figure 3(a). Note; the principal eigenvalue has no unit. The colors of these areas seem to be uniform, and however the magnitudes have some differences. The eigenvalues of EIA and other non-earthquake background noises are small. It shows that the results of 2DPCA are not affected by the EIA and other non-earthquake background noises compared with the results of Figure 1(b).

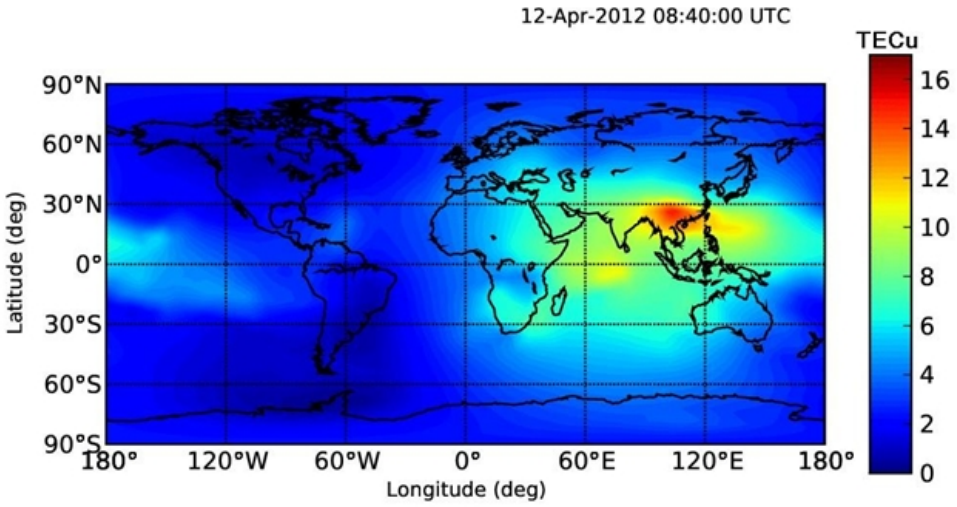

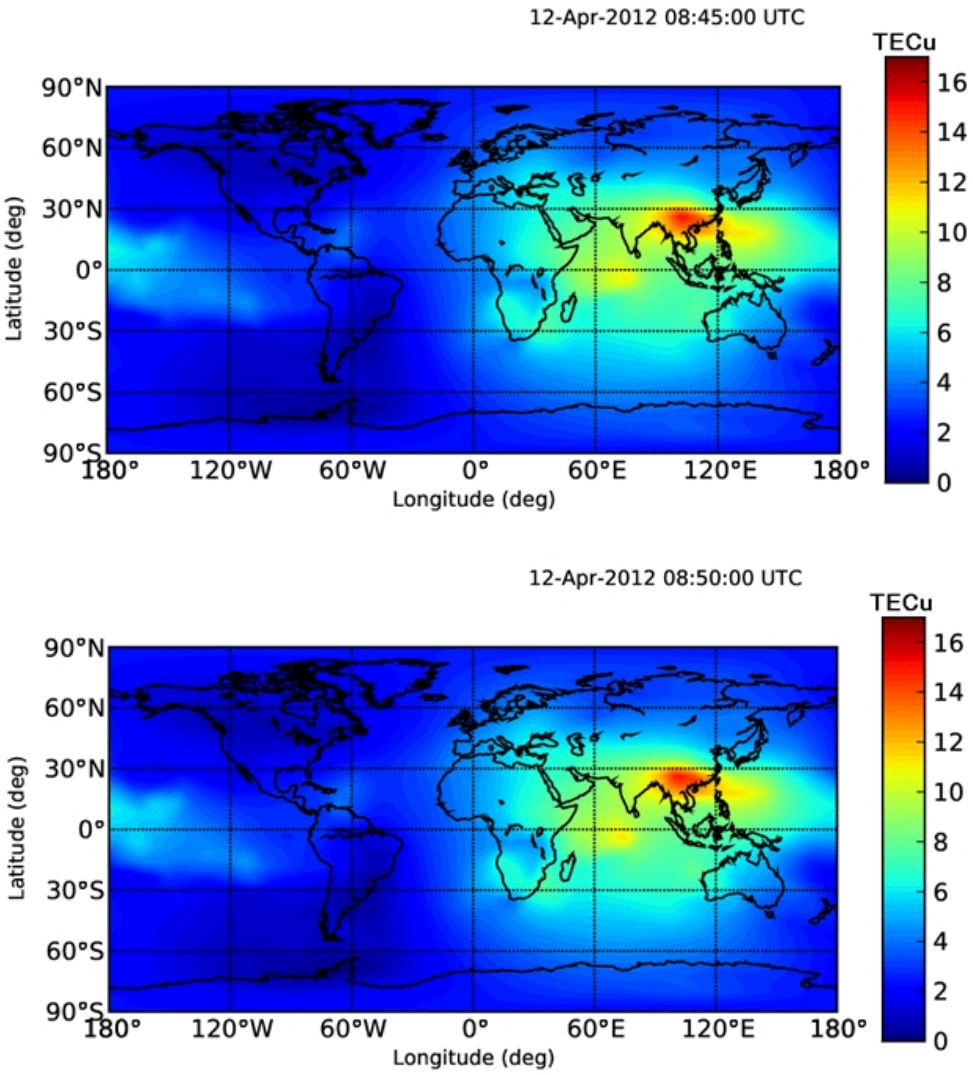

Fig. 4(a). The figures show the GIMs at the time 08:40 to 08:50 UT on 12 April 2012. The equatorial ionization anomaly (EIA) crests of dense GPS TEC bands at low latitudes centered about 30°N and 10°S geographic latitudes straddle the geomagnetic equator and range from about 70°E to 120°E.

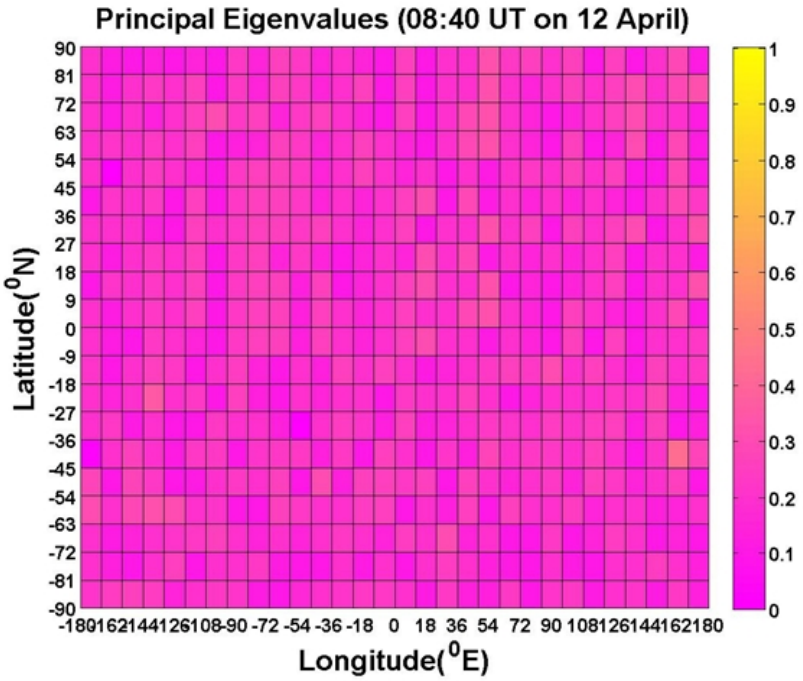
Principal Eigenvalues (08:40 UT on 12 April)
Latitude(0N)
90 81 72 63 54 45 36 27 18 9 0 -9 -18 -27 -36 -45 -54 -63 -72 -81 -90
-180 -162 -144 -126 -108 -90 -72 -54 -36 -18 0 18 36 54 72 90 108 126 144 162 180
Longitude(0E)
1 0.9 0.8 0.7 0.6 0.5 0.4 0.3 0.2 0.1 0

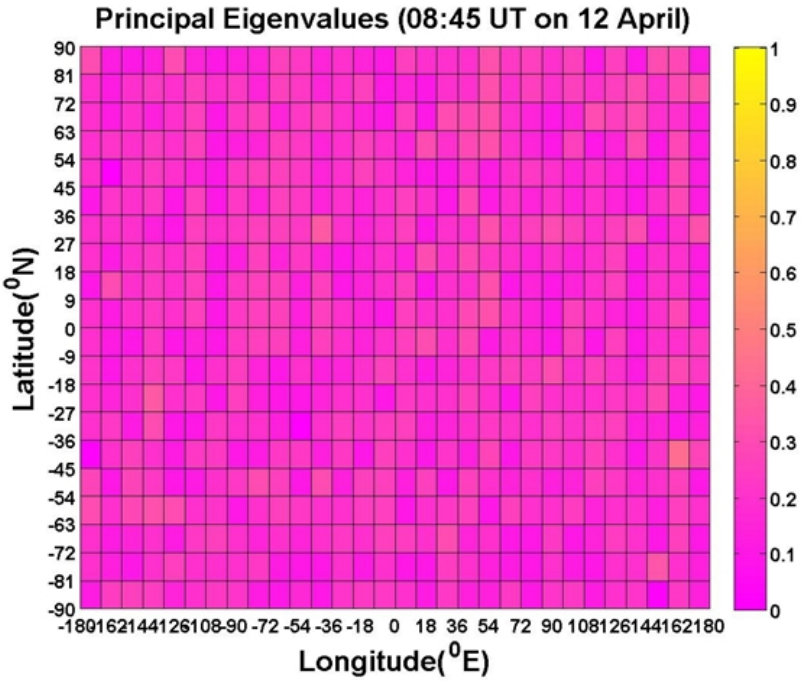
Principal Eigenvalues (08:45 UT on 12 April)
Latitude(0N)
90 81 72 63 54 45 36 27 18 9 0 -9 -18 -27 -36 -45 -54 -63 -72 -81 -90
-180 -162 -144 -126 -108 -90 -72 -54 -36 -18 0 18 36 54 72 90 108 126 144 162 180
Longitude(0E)
1 0.9 0.8 0.7 0.6 0.5 0.4 0.3 0.2 0.1 0

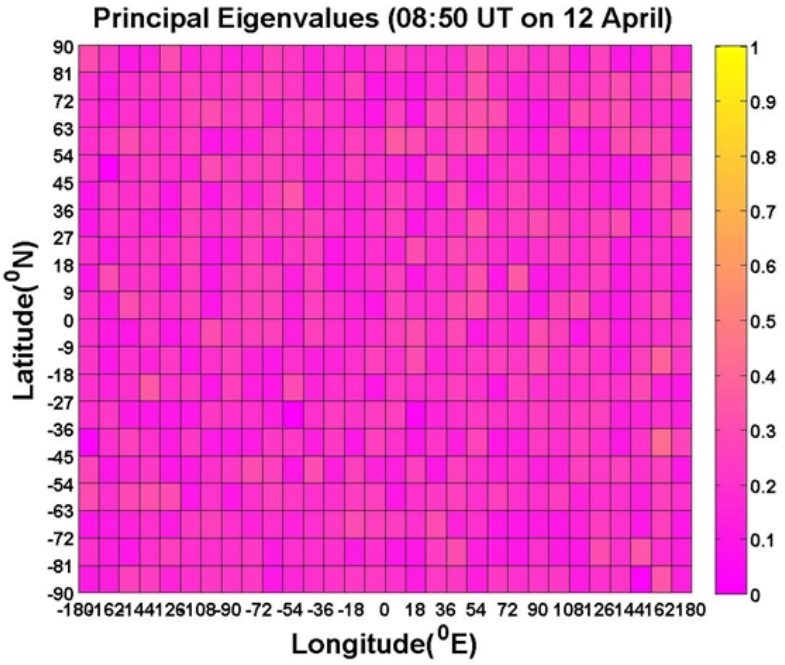

Fig. 4(b). The figures give a color-coded scale of the magnitudes of principal eigenvalues using 2DPCA related to Figure 4(a).

To get a clear understanding of the relative effects of the geomagnetic storm on the outcomes of 2DPCA applied to ionospheric TEC in the discovery of earthquake-related TEC anomalies, 2DPCA is applied to the TEC data of GIMs at the time 01:15 to 01:35 UT on 28 February 2012 with a geomagnetic storm. This experiment will provide principal eigenvalues for TEC anomalies under geomagnetic conditions and these principal eigenvalues can be used for comparison with principal eigenvalues given by 2DPCA analysis of this earthquake. For this experiment, 2DPCA is applied to study the impact of geomagnetic storm on TEC in the ionosphere. On 28 February 2012 was followed by a geomagnetic storm according to Kp indices shown in Figure 5. The TEC data of GIMs at 01:15 to 01:35 UT in Figure 6(a) are processed using 2DPCA with same method described in section 2.2. The EIA is not easy to observe due to a geomagnetic storm in the GIMs. The results are represented in Figure 6(b) with the magnitude of principal eigenvalues being small. Even a geomagnetic storm influence on the ionosphere did not produce the same level of large principal eigenvalues returned by 2DPCA for TEC anomalies. This is a strong indication that 2DPCA is surely suitable for in detecting earthquake-related TEC anomalies for large earthquakes rather than PCA.

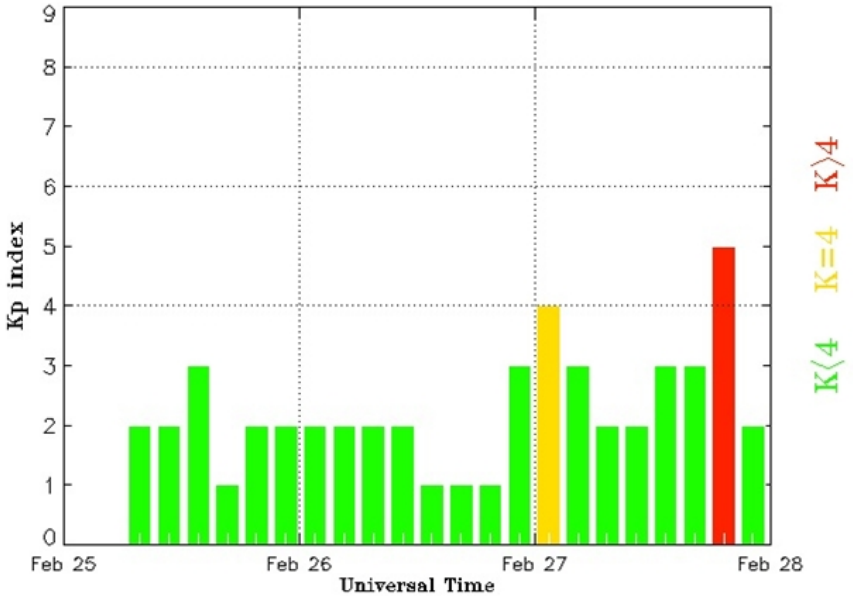

Fig. 5. This figure shows the Kp indices from 07 to 09 March 2012 (NOAA Space Weather Prediction Center).

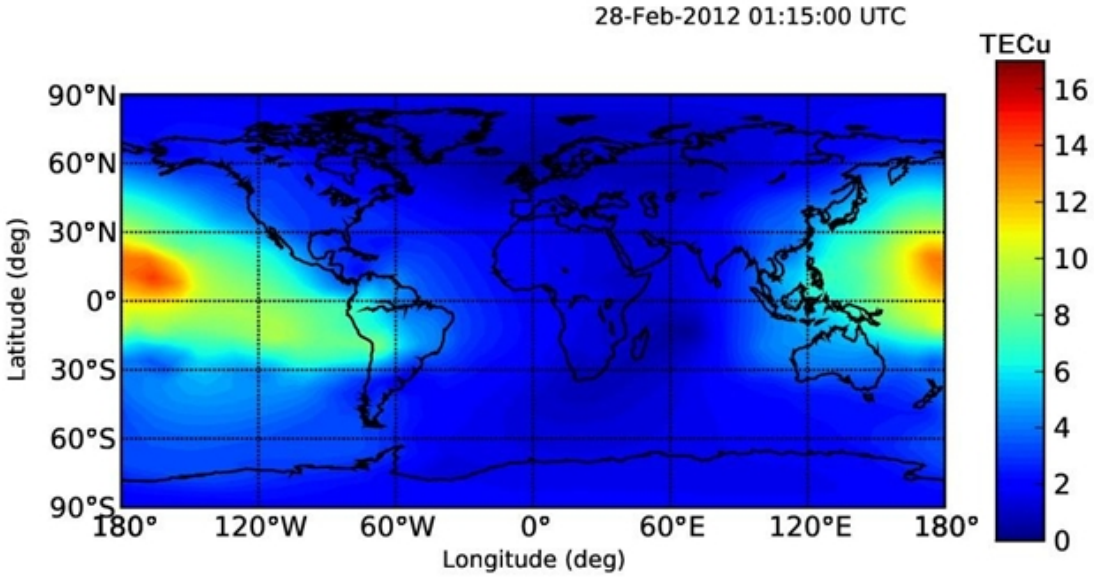

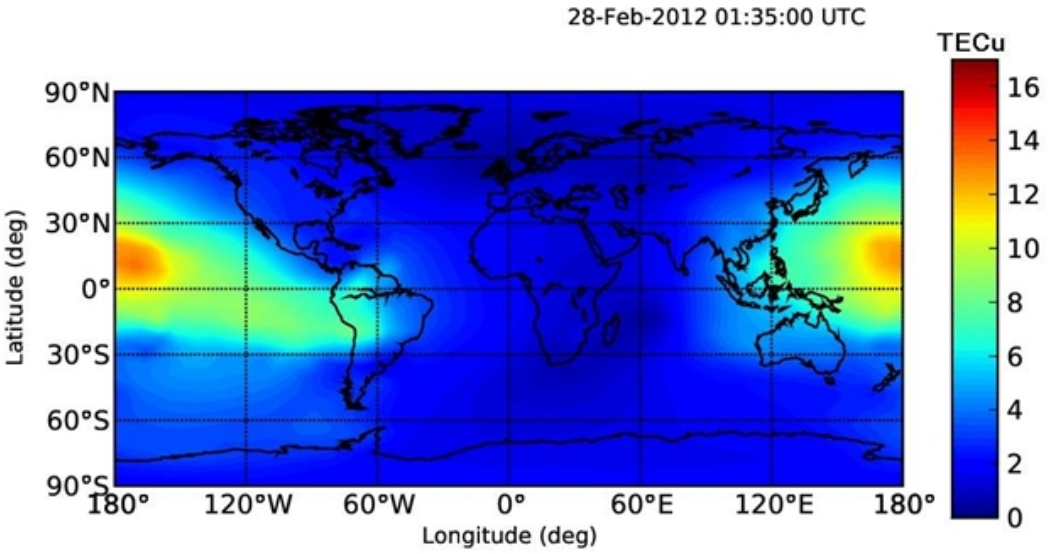

Fig. 6(a). The figures show the GIMs at the time 01:15UT to 01:35 on 28 February 2012. The EIA is not easy to observe due to a geomagnetic storm in this GIM.

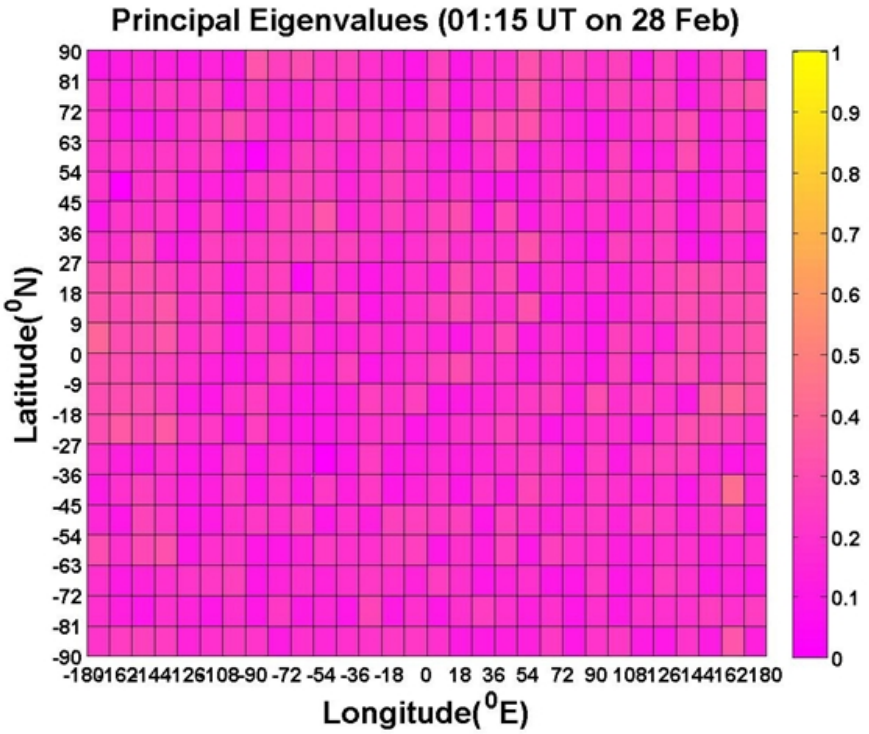

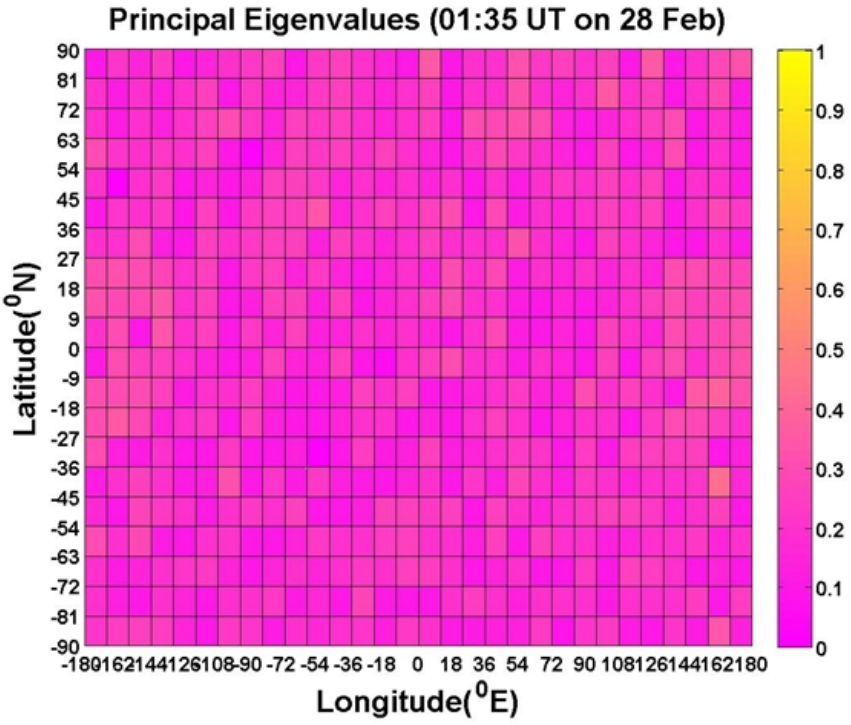

Fig. 6(b). The figures give a color-coded scale of the magnitudes of principal eigenvalues using 2DPCA related to Fig. 6(a).

The TEC data of GIMs after 08:40 UT are examined using 2DPCA to estimates the duration time of TEC anomaly related to this earthquake. The earthquake-associated TEC anomaly for GIM at 08:45 UT (Figure 7a) released in the same region but with less intensity (Fig. 7b). For the GIM at 08:50 (Figure 8a), no earthquake-associated TEC anomaly occurred (Figure 8b). Results show that the duration time is at least 5 minute (300 s). To show the credibility to estimate the duration time of earthquake-related TEC anomaly in this study (~5 minutes), [1] researched shock acoustic wave due to occurring of the earthquakes to affect ionosphere. They studied the earthquake effects in Turkey on 17 August and 12 November 1999 and in Southern Sumatra on 04 June 2000 and found the ionospheric response related to the earthquakes due to shock acoustic wave is 180-390 s.

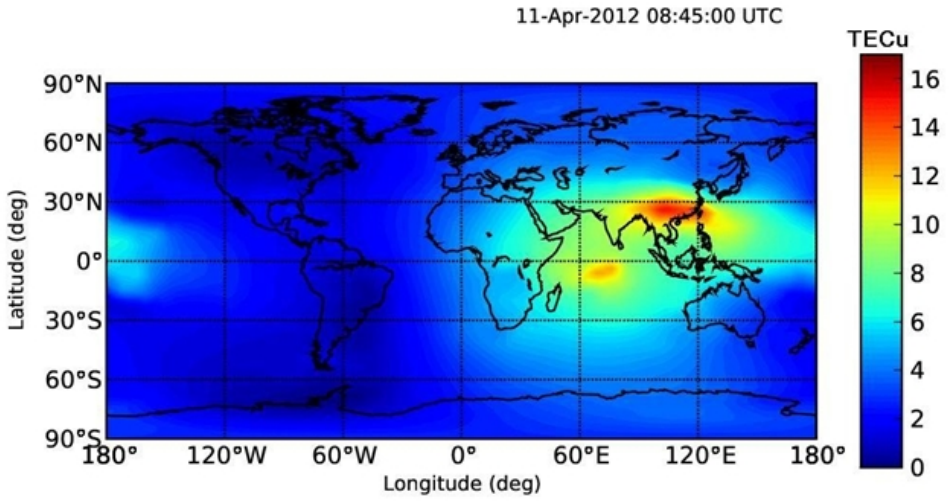

Fig. 7(a). This figure shows the GIM at the time 08:45UT on 11 April. Two equatorial ionization anomaly (EIA) crests of dense GPS TEC bands at low latitudes centered about 30°N and 10°S geographic latitudes straddle the geomagnetic equator and range from about 60°E to 130°E.

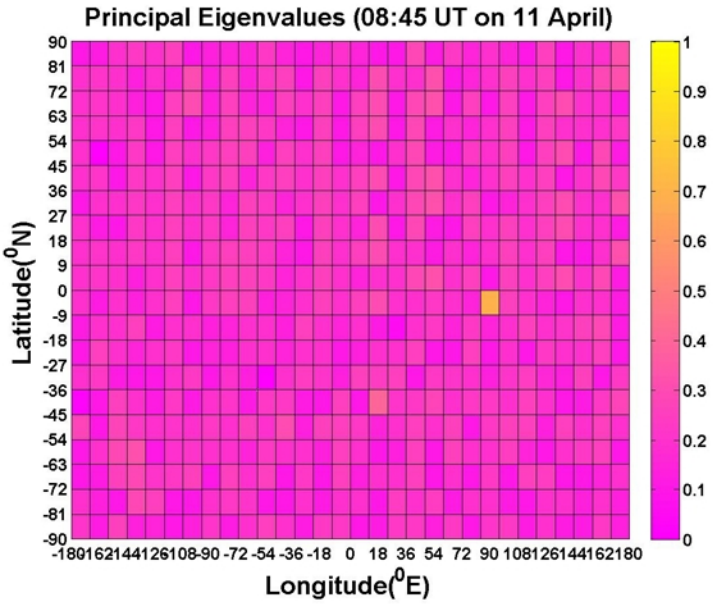

Fig. 7(b). The figure gives a color-coded scale of the magnitudes of principal eigenvalues of 2DPCA corresponding to Figure 7(a). The earthquake-related TEC anomalies are represented using large principal eigenvalues being 0.71

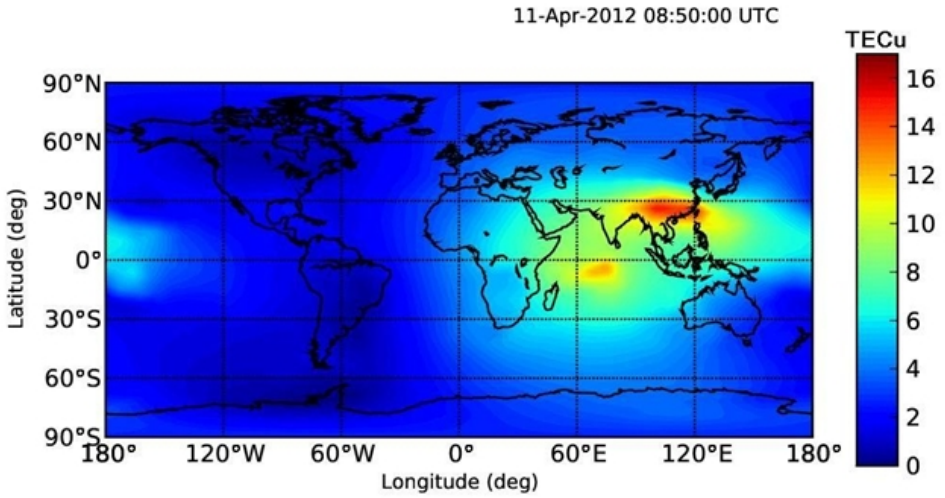

Fig. 8(a). This figure shows the GIM at the time 08:50UT on 11 April. The equatorial ionization anomaly (EIA) crests of dense GPS TEC bands at low latitudes centered about 30°N and 10°S geographic latitudes straddle the geomagnetic equator and range from about 60°E to 130°E.

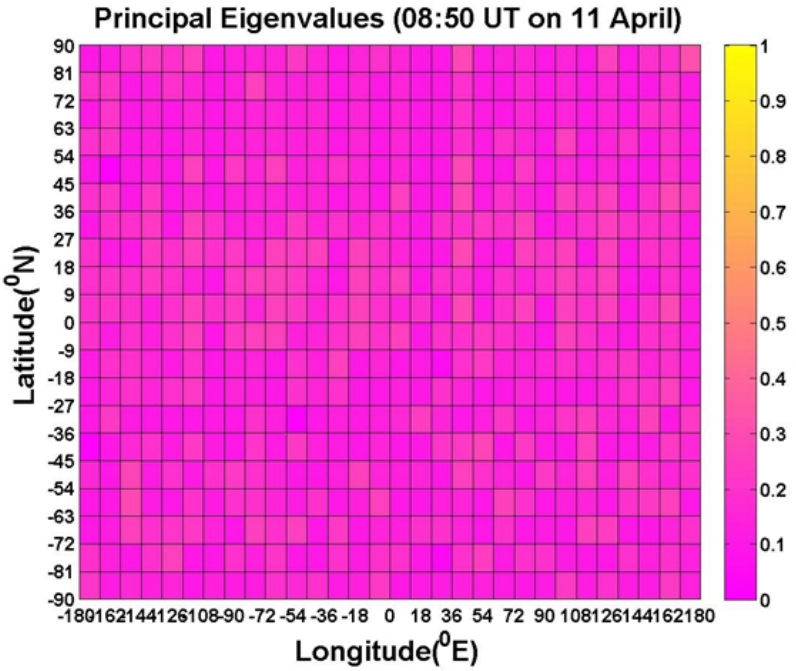

Fig. 8(b). The figure gives a color-coded scale of the magnitudes of principal eigenvalues of 2DPCA corresponding to Figure 8(a). No earthquake-associated TEC anomaly occurred.

2DPCA was able to detect a TEC anomaly related to the 11 April 2012 Indonesia's Sumatra earthquake at the time 08:40 to 08:45 UT while the earthquake occurred at 08:38:37UT. Identifying the precise cause of earthquake related TEC anomalies was not easy. One reason for this is the number of potential causes of earthquake related TEC anomalies that arise during earthquake preparation, the mainshock, and aftershocks. For example during the earthquake preparation phase, [33] suggested that radon emanating from active faults and cracks before earthquakes ionize the near ground atmosphere to produce large vertical electric fields. [7] proposed that mobile positive holes in the earth's crust could be activated by low-energy impact, sound waves, and micofractures, creating charge clouds that could explain electromagnetic activity. Gravity waves arising from fine vibrations in the earth's surface leading to gas release are another possibility and this resulted in lower atmospheric turbulence and eventual ionospheric perturbations [28]. However, once an earthquake has occurred then the most evident physical mechanism is ground motion and fine surface vibrations. The noted anomaly in this study began at an altitude of the F-region (the height above 150km) of the ionosphere. Accordingly, studies of electromagnetic disturbance suggested two possible explanations for earthquake associated anomalies at this altitude. One is acoustic gravity waves caused by Joule heating [14] and the other is the presence of an electric field creating large scale ionospheric density irregularities [23,32] coupled with potential drift of the anomaly toward the equator. However, this anomaly resembles what one would expect from rising acoustic gravity waves because of strong motion. Large earthquake could produce a stark acoustic shock wave of great amplitude by the time it reaches the ionosphere. Such a description could possibly represent the stark and concentrated energy of an acoustic shockwave being formed in the lower atmosphere after the earthquake traveling up into the ionosphere [18]. Therefore this is the possibility described in the introduction to this paper whereby high speed slanted acoustic shock wave, which had small horizontal component, caused by stark strong motion at the earth's surface are amplified through the atmosphere to affect TEC in the ionosphere from the earthquake zone. The TEC anomaly might be TEC a density variance. The duration time of earthquake-related TEC anomaly was estimated at least 5 minutes from the time 08:40 to 08:45 UT. 2DPCA was tool in future analysis of earthquakes and related TEC phenomena with two-dimensional SSS TEC data. The results were not affected by geomagnetic storm in the detection of earthquake-related TEC anomalies.

5. CONCLUSION

2DPCA had the advantage over PCA to detect the TEC anomaly related to the 11, April 2012 Indonesia's Sumatra earthquake. Results have shown that a local ranging TEC anomaly was detectable from the time 08:40 to 08:45 UT. The earthquake-related TEC anomaly could be indicative of a rising high speed slanted acoustic shock wave, which had small horizontal component, so that the earthquake-related TEC anomaly range is outside the epicenter of this earthquake and it might be a TEC density variance with the duration time is at least 5 minutes.

ACKNOWLEDGEMENTS

The author is grateful to: NASA Global Differential GPS system for their useful references Data.

COMPETING INTERESTS

Authors have declared that no competing interests exist.

REFERENCES

1. Afraimovich EL. Perevalova NP, Plotnikov AV, Uralov AM, The shock-acoustic waves generated by earthquakes. Annales Geophysicae. 2001;19:395-409
2. Artru J, Lognonné P,: Normal modeling of post-seismic ionospheric oscillations. Geophysical Research Letter. 2001;28(4):697-700.
3. Bartels J, Heck NH, Johnston HF, The three-hour range index measuring geomagnetic activity, Geophys. Res. 1939;44,411-454.
4. Chen K, Gao Y, Real-Time Precise Point Positioning Using Single Frequency Data. ION GNSS 2005, Long Beach, CA, USA; 2005
5. Elsner, J.B and S. P. Kavlakov, 2001, Hurricane intensity changes associated with geomagnetic variation. Atmospheric Science Letters (2001). doi:10.1006/asle.2001.0040
6. Földiák P. Adaptive Network for Optimal Linear Feature Extraction,'' Int. Joint Conf. on Neural Networks, Washington, DC, I, 401.1989,
7. Freund F, Time-resolved study of charge generation and propagation in igneous rocks. Journal of Geophysical Research, 2000;105,11001-11019.
8. Freund F, Rocks T, That Crackle and Sparkle and Glow Strange Pre-Earthquake Phenomena. Journal of Scientific Exploration, 2003;17(1),37-71.
9. Gao Y and K. Chen, 2006, Development of a Real-Time Single-Frequency Precise Point Positioning System and Test Results. ION GNSS 19th International Technical Meeting of Satellite Division, 26-29 September 2006, Fort Worth, TX
10. Garcia R, Crespon F, Ducic, Lognonné VP,. Three-dimensional ionospheric tomography of post-seismic perturbations produced by the Denali earthquake from GPS data. Geophys. J. Int. 2005;163,1049–1064.
11. Jeff. MA future Space Weather catastrophe : a disturbing possibility. 2012
12. Jeong DH, Ziemkiewicz C, Ribarsky W, Chang R, Understanding Principal Component Analysis Using a Visual Analytics Tool. Charlotte Visualization Center, UNC Charlotte. 2009.
13. Hamilton DC, Gloeckler G, Ipavich FM, Studemann W, Wilken B, Kremser G, , Ring current development during the great geomagnetic storm of February. J. Geophys. Res. 1986;93,14343.
14. Hegai VV, Kim V P, Nikiforova L I, A possible generation mechanism of acoustic-gravity waves in the ionosphere before strong earthquakes. J. Earthquake Predict. Res, 1997;6,584-589.
15. Hegai VV, Kim VP, Liu JY, The ionospheric effect of atmospheric gravity waves excited prior to strong earthquake. Advances in Space Research, 2006;37,653-659.
16. Hernández-Pajares M, Juan JM, Sanz J, Orus R, Garcia-Rigo A,· Feltens J, Komjathy A, Schaer SC and Krankowski A, 2009, The IGS VTEC maps: a reliable source of ionospheric information since. J Geod. 1998;83:263–275. DOI 10.1007/s00190-008-0266-1
17. Hobara Y, Parrot M. Ionospheric perturbations linked to a very powerful seismic event. Journal of Atmospheric and Solar-Terrestrial Physics. 2005;67:677-685
18. Jin S, Zhu W, Afraimovich E.. Co-seismic ionospheric and deformation signals on the 2008 magnitude 8.0 Wenchuan Earthquake from GPS observations. International Journal of Remote Sensing. 2010;31:(13):3535-3543.

19. Kechine MO, Tiberius CCJM, vander Marel H. Real-time Kinematic Positioning with NASA's Global Differential GPS System. GNSS Conference, St. Petersburg, Russia; 2004.
20. Kong H, Wang L, Teoh EK, Li X. Wang JG, Venkateswarlu R, Generalized 2D principal component analysis for face image representation and recognition. Neural Networks. 2005;18:585–594
21. Kramer MA. Nonlinear Principal Component Analysis Using Autoassociative Neural Networks. AIChe Journal. 1991;37(2):233-243.
22. Lin JW, Ionospheric total electron content (TEC) anomalies associated with earthquakes through Karhunen-Loéve Transform (KLT). Terrestrial, Atmospheric and Oceanic Sciences. 2010;21:253-265.
23. Liu JY, Chuo YJ, Shan SJ, Tsai YB, Pulinets SA, Yu SB. Pre-earthquake ionospheric anomalies monitored by GPS TEC. Annales Geophys. 2004;22:1585-1593.
24. Liu JY, Chen YI, Chuo YJ, Chen CS. A statistical investigation of pre-earthquake ionospheric anomaly. Journal of Geophysical Research. 111, A05304,10.1029/ 2005JA011333. 2006.
25. Liu JY, Chen YI. Chen CH, Liu CY, Chen CY, Nishihashi M. Li J Z, Xia YQ, Oyama KI, Hattori K, Lin. Seismoionospheric GPS total electron content anomalies observed before the CH 12 May 2008 Mw=7.9 Wenchuan Earthquake. Journal of Geophysical Research. 2009;114. Doi: 10.1029/2008JA013698.
26. Lognonné P, Artru J, Garcia R, Crespon F, Ducic V, Jeansou E, Occhipinti G, Helbert J, Moreaux G, Godet PE. Ground-based GPS imaging of ionospheric post-seismic signal. Planetary and Space Science 54. 2006;528-540.
27. Marchand R, Berthelier JJ, Simple model for post seismic ionospheric disturbances above an earthquake epicentre and along connecting magnetic field lines. Nat. Hazards Earth Syst. Sci. 2008;(8)1341–1347
28. Molchanov OA, Hayakawa M. Subionospheric VLF signal perturbations possibly related to earthquakes. Journal of Geophysical Research. 1998;103(8):17489-17504,
29. Mukherjee GK. Storm-associated Variations of [OI] 630.0 nm Emissions from Low Latitudes. Terrestrial. Atmospheric. Oceanic. Sciences. 1999;10(1):265-276.
30. Ouyang G, Wang J, Wang J, Cole D, Analysis on Temporal-Spatial Variations of Australian TEC. International Association of Geodesy Symposia. 2008;133(4):751-758, DOI: 10.1007/978-3-540-85426-5_86
31. Pulinets SA., Boyarchuk KA, Hegai V V, Kim VP, Lomonosov AM, , Quasielectrostatic model of atmosphere-thermosphereionosphere coupling, Advances in Space Research. 2000;26(8):1209–1218.
32. Pulinets SA., Legen'ka AD, Spatial-temporal characteristics of the large scale disturbances of electron concentration observed in the F-region of the ionosphere before strong earthquakes. Cosmic Res. 2003;41,221-229.
33. Pulinets S, Boyarchuk K. Ionospheric Precursors of Earthquakes. Springer-Verlag, Berlin, Heidelberg; 2004.
34. Pulinets SA. Ionospheric Precursors of Earthquakes; Recent Advances in Theory and Practical Applications. Terrestrial. Atmospheric. Oceanic. Sciences. 2004;15(3):413-435.
35. Pulinets SA, Kotsarenko N, Ciraolo L. Pulinets IA. Special case of ionospheric day–to-day variability associated with earthquake preparation. Advances in Space Research. 2007;39(5):970-977.
36. Sanguansat P. Principal Component Analysis, Published by InTech, Janeza Trdine 9, 51000 Rijeka, Croatia. 2012;300.

37. Singh RP, Mehdi W, Gautam R, Senthil Kumar J, Zlotnick J, Kafatos M. Precursory signals using satellite and ground data associated with the Wenchuan Earthquake of 12 May 2008. International Journal of Remote Sensing. 2010;31(13)3341-3354.
38. Yang J, Zhang D, Frangi AF, Yang JY. Two-dimensional PCA: a new approach to appearance-based face representation and recognition. IEEE Transactions on Pattern analysis and Machine Intelligence. 2004;26(1):131-137.
39. Zhao B, Yu T, Wang M, Wan W, Lei J, Liu L, Ning B. Is an unusual large enhancement of ionospheric electron density linked with the 2008 great Wenchuan earthquake? Journal of Geophysical Research. 2008;113:A11304. doi: 0.1029/2008JA013613.

Peer-review history:
The peer review history for this paper can be accessed here:
http://www.sciencedomain.org/review-history.php?iid=290&id=22&aid=2275